

# Pulsed LD side-pumped MgO: LN electro-optic cavity-dumped 1123 nm Nd: YAG laser with short pulse width and high peak power

Yang Bai<sup>1,2,3</sup>, Bing Bai<sup>1,2,3</sup>, Diao Li<sup>1,2,3</sup>, Yanxiao Sun<sup>1,2,3</sup>, Jianlin Li<sup>1,2,3</sup>, Lei Hou<sup>1,2,3</sup>,  
Mingxuan Hu<sup>1,2,3</sup>, and Jintao Bai<sup>1,2,3</sup>

<sup>1</sup>National Key Laboratory of Photoelectric Technology and Functional Materials (Culture Base), Institute of Photonics and Photon-Technology, Northwest University, Xi'an 710069, China

<sup>2</sup>Shaanxi Engineering Technology Research Center for Solid State Lasers and Application, Xi'an 710069, China

<sup>3</sup>Provincial Key Laboratory of Photo-electronic Technology, Institute of Photonics and Photon-Technology, Northwest University, Xi'an 710069, China

(Received 12 November 2017; revised 29 November 2017; accepted 19 December 2017)

## Abstract

We report a cavity-dumped 1123 nm laser with narrow pulse width and high peak power by an MgO: LN crystal electro-optic (EO) modulator. Based on the structural optimization design of a folded biconcave cavity using the 808 nm pulsed laser diode (LD) side-pumped ceramic Nd: YAG rod, output pulses with maximum pulse energy and peak power up to 39.6 mJ and 9.73 MW were obtained, corresponding to 100 Hz repetition rate and 4.07 ns pulse width. The instabilities of pulse width and pulse energy were  $\pm 1.55\%$  and  $\pm 2.06\%$ , respectively. At the highest repetition rate of 1 kHz, the pulse energy, pulse width, and peak power were 11.3 mJ, 5.05 ns, and 2.24 MW, respectively. The instabilities of pulse width and pulse energy were  $\pm 2.65\%$  and  $\pm 3.47\%$ , respectively.

**Keywords:** cavity-dumped; high peak power; MgO: LN EO; 1123 nm laser; short pulse width

## 1. Introduction

In recent years, pulsed Nd: YAG lasers with high energy, narrow pulse width, high peak power and good stability have been widely used in laser radar, precision machining, optical communications, ranging, medicine, nonlinear optical frequency conversion, and so on<sup>[1–5]</sup>. The polycrystalline ceramic Nd: YAG emerges as promising laser gain medium for high energy, high power all solid-state lasers. It has similar properties with Nd: YAG crystal in terms of upper-level lifetime, absorption cross section, extinction ratio and thermal conductivity. Moreover, ceramic Nd: YAG has advantages of simple fabrication process, low cost, high doping concentration and easy batch production<sup>[6–11]</sup>. Generally, there are three laser radiations in ceramic Nd: YAG, which emit wavelengths at 1318, 1064, and 946 nm corresponding to energy transition states from the Stark levels of the upper laser state  $^4F_{3/2}$  to three individual lower laser states of  $^4I_{13/2}$ ,  $^4I_{11/2}$  and  $^4I_{9/2}$ . However, the least energetic

transition in the manifold  $^4F_{3/2}$  to  $^3I_{11/2}$  corresponds to another wavelength at 1123 nm of ceramic Nd: YAG<sup>[12]</sup>. The 1123 nm laser has attracted particular interest of researchers because of its wide applications in many special fields. For example, it can be used as a pumping source for thulium up-conversion fiber lasers to generate the laser emission<sup>[13]</sup>, or for space remote sensing<sup>[14]</sup>. In addition, 1123 nm laser can also be used to produce 561 nm yellow laser by frequency doubling, which has become the ideal light source in photodynamic therapy for cutaneous hemangioma and micro-venous malformations<sup>[12, 15–17]</sup>.

At present, investigations on pulsed 1123 nm laser mainly focus on passively Q-switched output based on saturable absorber or self-mode-locked output. In 2016, Li *et al.* obtained a passively Q-switched 1123 nm laser with a repetition rate of 116 kHz, pulse width of 8 ns, and single-pulse energy of 69  $\mu$ J by using 808 nm laser diode (LD) end-pumped ceramic Nd: YAG and Cr<sup>4+</sup>: YAG saturable absorber<sup>[18]</sup>. In 2017, Bai *et al.* reported a passively Q-switched 1123 nm laser with a pulse repetition rate of 457 kHz, pulse width of 231 ns, and single-pulse energy of 0.38  $\mu$ J by using 808 nm LD end-pumped ceramic Nd:

Correspondence to: Y. Bai, Institute of Photonics and Photon-Technology, Northwest University, Xi'an 710069, China. Email: [by@nwu.edu.cn](mailto:by@nwu.edu.cn)

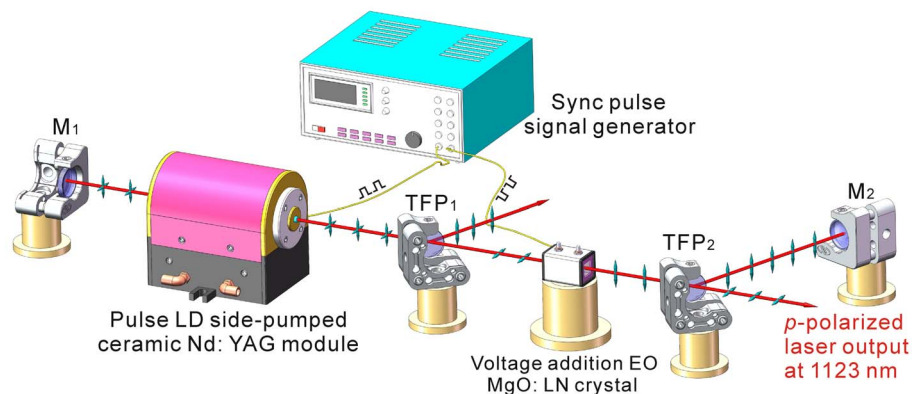


Figure 1. Schematic of the laser setup.

YAG and gold nanotriangle saturable absorber<sup>[19]</sup>. In 2017, Sung *et al.* obtained a self-mode-locked Nd:YAG laser at 1123 nm with a repetition rate of 4.5 GHz, pulse width of 50.8 ps, and single-pulse energy of 0.53 nJ by using 808 nm LD end-pumped Nd:YAG crystal<sup>[20]</sup>. In the above methods, LD end-pumped short Nd:YAG does not provide high laser gain for 1123 nm stimulated radiation. Although passive saturable absorbers can be used to compress pulse width, the low optical damage threshold of these materials hinders the acquisition of laser pulses with high energy and high peak power. The pulse width of self-mode-locked laser at 1123 nm has been reduced to be about 50 ps, but the single-pulse energy still remains a few nano-joules to tens of micro-joules, and the peak power is only a few to a few tens of kilowatts. Because of the upper-level lifetime of the gain media and the light transmittance of the output mirrors, traditional actively Q-switched lasers based on upper-level energy storage in gain media are also difficult to control and get stable laser pulses with width shorter than 5 ns due to the changes of repetition rate. It is required that the corresponding pulse energy is greater than 10 mJ, the peak power is greater than 2 MW, and the instability is less than  $\pm 2.65\%$  at a repetition rate of 1 kHz. Based on the principle of intracavity photon energy storage, the laser pulse width obtained by using the cavity-dumping technique is only related to the length of cavity and the rising edge of the modulation switch<sup>[21–23]</sup>. Therefore, it is possible to realize the output of 1123 nm pulsed laser with high single-pulse energy ( $> \text{mJ}$ ), short pulse width ( $< 5 \text{ ns}$ ) and high peak power ( $> \text{MW}$ ) via LD side pumping.

In this paper, for the first time, to the best of our knowledge, we demonstrate a cavity-dumped 1123 nm laser. Output pulses with repetition rates varying from 100 Hz to 1 kHz, pulse width shorter than 5 ns and peak power from 2 MW to 10 MW were obtained by utilizing 808 nm pulsed LD side-pumped ceramic Nd:YAG rod and electro-optical (EO) cavity dumping.

## 2. Laser setup and operation principle

The schematic of the EO cavity-dumped 1123 nm laser is shown in Figure 1. A ceramic Nd:YAG rod ( $\varphi 3 \times 65 \text{ mm}$ , with 0.6 at.%  $\text{Nd}^{3+}$  concentration) was used as a gain medium for obtaining 1123 nm laser in the experiment. The ceramic Nd:YAG rod was side-pumped by three 808 nm pulsed LD arrays distributed in  $120^\circ$  angle mutually, and its two end surfaces were anti-reflection (AR) coated for wavelengths from 1064 nm to 1319 nm (reflectance  $R < 0.5\%$ ). Since the stimulated emission cross section for the 1123 nm transition is approximately 15 times smaller than that for the 1064 nm emission<sup>[24]</sup>, an indispensable criterion to obtain laser emission at 1123 nm is to suppress the competing transitions at 1064, 1319, 1112 and 1116 nm. In the experiment, a multi-layered high-transmission coating in the cavity mirrors was needed.  $M_1$  and  $M_2$  are plano-concave mirrors. The plane side of mirror  $M_1$  was AR coated for wavelengths from 1064 nm to 1319 nm ( $R < 0.5\%$ ), and its concave side was high reflection (HR) at 1123 nm ( $R > 99.7\%$ ), and AR coated at 1064 nm ( $R < 5.5\%$ ), 1319 nm ( $R < 6.2\%$ ), 1112 nm ( $R < 92.4\%$ ) and 1116 nm ( $R < 93.4\%$ ). The concave side of the mirror  $M_2$  was HR coated at 1123 nm ( $R > 99.7\%$ ), and AR coated at 1064 nm ( $R < 5.9\%$ ), 1319 nm ( $R < 6.7\%$ ), 1112 nm ( $R < 92.6\%$ ) and 1116 nm ( $R < 93.6\%$ ), and its plane side was AR coated from 1064 nm to 1319 nm ( $R < 0.6\%$ ).

To date, traditional crystals such as  $\text{BaB}_2\text{O}_4$  (BBO),  $\text{KH}_2\text{PO}_4$  (KDP),  $\text{RbTiOPO}_4$  (RTP) and  $\text{LiNbO}_3$  (LN) have been extensively used for EO modulation in solid-state lasers. Nonetheless, BBO and KDP are hygroscopic, RTP is expensive, and LN crystal has low optical damage threshold. In contrast with traditional LN crystal, the magnesium oxide doped LN crystal (MgO:LN) has comparative half wave voltage of transverse electro-optic modulation, and its optical damage threshold is increased by two orders of magnitude<sup>[25, 26]</sup>. Especially, low price makes it an

advantageous candidate against the other EO crystals. Therefore, an MgO: LN crystal (20 mm<sub>(length)</sub> × 7 mm<sub>(width)</sub> × 7 mm<sub>(thickness)</sub>, 5.0 mol.% MgO doping, 200 MW optical damage threshold) was used for transverse EO modulation, which was AR coated for 1123 nm ( $R < 0.5\%$ ). It was driven by an EO switch with a rising edge shorter than 4 ns at 10 Hz, a repetition rate tuning range from 1 Hz to 2.0 kHz and a dynamic–static ratio of 0.9 : 1. The triggering signals of the pulsed LD and EO switch were received from the same delay pulse generator. Delay triggering time of the two signals was adjusted to ensure that the emission of the 808 nm pulse LD was synchronized with the voltage adding of MgO: LN crystal. The TFP<sub>1</sub> and TFP<sub>2</sub> were Brewster plane mirrors for 1123 nm light.

The 1123 nm randomly polarized laser emission produced by the ceramic Nd: YAG rod was split into a bunch of reflected s-polarized light and another bunch of transmitted p-polarized light by the TFP<sub>1</sub>. When the EO crystal MgO: LN was not loaded with half wave voltage, the cavity was at static state. At this point, the s-polarized 1123 nm light reflected by TFP<sub>1</sub> and the p-polarized 1123 nm light (passing through TFP<sub>1</sub>, EO crystal MgO: LN and the TFP<sub>2</sub>) propagated directly out of the cavity without stimulated oscillation. Next, when the transverse half wave voltage was abruptly loaded on the EO MgO: LN crystal, the cavity was at dynamic state. The polarized state of 1123 nm light passing through the MgO: LN crystal was switched from p to s. The s-polarized 1123 nm light reflected by the TFP<sub>2</sub> was amplified by stimulated oscillation without output between M<sub>1</sub> and M<sub>2</sub>, so that the photon energy of 1123 nm laser was stored in the cavity. Finally, when the half wave voltage was removed, the laser cavity turned to static state, and then a p-polarized 1123 nm laser pulse was directly output through the TFP<sub>2</sub>, corresponding to a transmittance close to 100%. It is worth noting that the laser pulse width is independent of the pulse repetition rate if the rising edge of the EO switch is fast enough, which should be equal to the round-trip time in the cavity  $\tau = 2L/c$ , where  $L$  is the optical length of cavity,  $c$  is the light speed in vacuum. If the rising edge of the EO switch is greater than  $2L/c$ , the output pulse width is determined by the rising edge. The actual polarizer is not always ideal. Un-polarized light transmitting through the polarizer is partially polarized rather than 100% linearly polarized. The ratio of the maximum transmitted light intensity to the minimum transmitted light intensity of the analyzer relative to the polarizer is defined as extinction ratio, which is an important parameter to measure the quality of the polarizer. The greater the extinction ratio is, the higher the polarization degree is. If the degree of polarization is not large enough, the continuous wavelength (CW) portion of the output light cannot be neglected. Therefore, the energy of the light pulse is reduced as the power of CW light increases. As a consequence, the combination of two Brewster plane mirrors and an EO crystal in this experiment is helpful to

improve the extinction ratio of the electro-optic modulator, so as to increase the polarization degree and pulse energy.

The thermal focal length of the gain medium can be reduced by the increase of pump power, which seriously affects the laser beam quality and stability, and even causes detuning of the laser oscillation. Therefore, it is necessary to optimize the structure of the cavity so that it has the characteristics of dynamic thermal insensitivity in the range of certain thermal focal length changes. When the pump current was increased from 50 A to 110 A, the measured thermal focal length (dynamic testing method) was reduced from ~430 mm to ~300 mm at 1 kHz, and from ~750 mm to ~620 mm at 100 Hz, respectively<sup>[27]</sup>. The structure of the cavity-dumped lasers is then optimized with ABCD matrix theory and the laser cavity analysis design software (LASCAD) by taking the measured thermal lens focal length into account<sup>[28]</sup>. The radii of concave curvature of the M<sub>1</sub> and the M<sub>2</sub> were ultimately calculated to be 2.5 m and 0.6 m, respectively. Optical length of the cavity was simulated to be 500 mm, corresponding to theoretical laser pulse width of 3.34 ns. When the thermal focal length of the cavity was reduced from 430 mm to 300 mm at 1 kHz, the corresponding stability factors of the sagittal and tangential beams were calculated by using the LASCAD software as follows:

$$\left| \frac{A_s + D_s}{2} \right| \approx 0.4054 \rightarrow 0.8671/1.0 \text{ kHz}, \quad (1)$$

$$\left| \frac{A_t + D_t}{2} \right| \approx 0.4652 \rightarrow 0.9167/1.0 \text{ kHz}, \quad (2)$$

where  $s$  and  $t$  represent sagittal and tangential beam spot, respectively. When the pulse repetition rate was 100 Hz, the thermal focal length was reduced from 750 mm to 620 mm, and the stability factors of the sagittal and tangential beams were calculated as follows:

$$\left| \frac{A_s + D_s}{2} \right| \approx 0.4932 \rightarrow 0.7432/100 \text{ Hz}, \quad (3)$$

$$\left| \frac{A_t + D_t}{2} \right| \approx 0.5417 \rightarrow 0.8266/100 \text{ Hz}. \quad (4)$$

Formulas (1)–(4) show that the stability parameters of the cavity are all smaller than 1 when the thermal focal length changes over a wide range at different pulse repetition rates. This confirms that the optimized cavity is insensitive to heat with the changes of the thermal focal length. At the maximum pump current of 110 A, the changes of the spot size at different positions in the resonant cavity are shown in Figures 2(a) and 2(b). The diameters of the sagittal and tangential beams at 1 kHz are calculated to be ~2.7 mm and ~2.6 mm in the ceramic Nd: YAG rod and the EO crystal MgO: LN, respectively. At 100 Hz, the spot diameters at the same location are 2.6 mm and 2.5 mm, respectively. The theoretical simulation shows that the difference between the

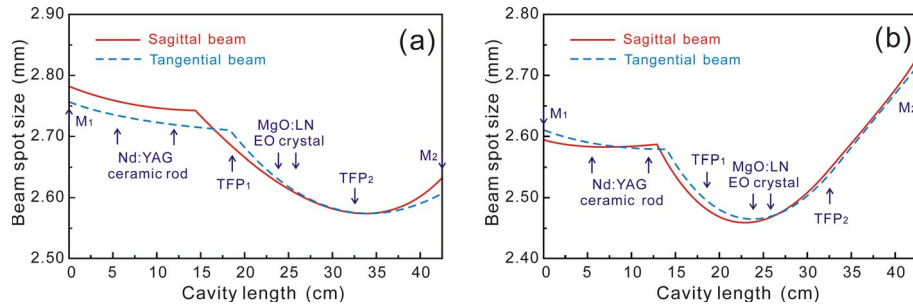


**Figure 2.** Variation curves of the sagittal and tangential spot sizes with the cavity length at repetition rates of (a) 1 kHz and (b) 100 Hz.

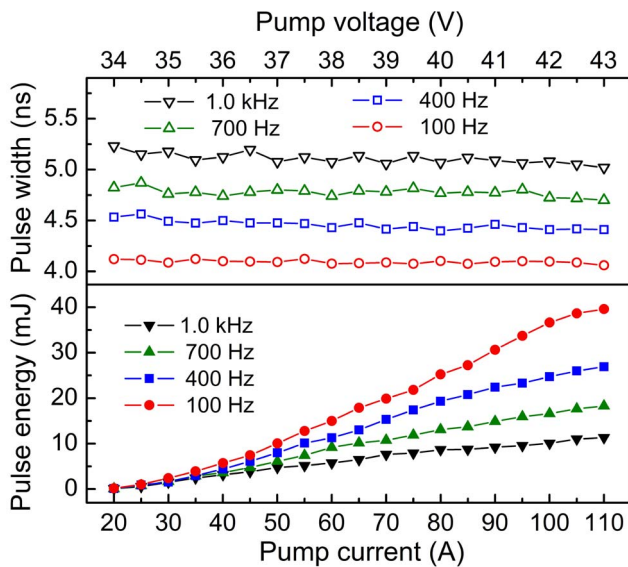


**Figure 3.** Pulse energy and pulse width as a function of pump current and pump voltage at different repetition rates.

spot sizes of the sagittal and tangential multi-mode beams is very small in the ceramic Nd: YAG rod and the EO crystal MgO: LN, which could improve the stability and beam quality of laser output<sup>[29]</sup>. The larger laser spot could also reduce the risk of light damage to ceramic Nd: YAG rod, MgO: LN crystal and optical coating.

### 3. Results and discussion

In the experiment, the transverse half wave voltage of the MgO: LN was  $4.2 \pm 0.2$  kV. The transverse half wave voltage and the delay time of the trigger signals were required to be finely tuned as the change of the pulse repetition rate. The changes of the single-pulse energy and the pulse width of the EO cavity-dumped 1123 nm laser with the pump current and pump voltage are shown in Figure 3 at different pulse repetition rates. It is demonstrated that the reduction of the pulse repetition rate leads to an increase of the one way laser gain under the same pump current,

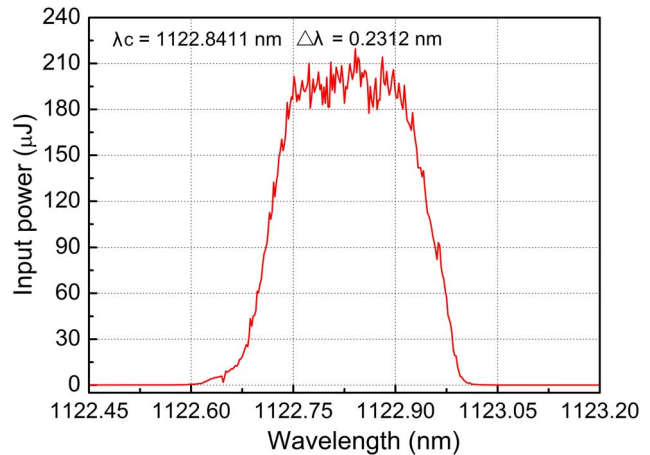


**Figure 4.** Output spectrum at 1 kHz repetition rate.

so that the single-pulse energy of the cavity-dumped lasers increases accordingly. With the increase of pump current, the fluctuation of the pulse width is smaller than  $\pm 0.1$  ns at the same pulse repetition rate. The peak power of the laser pulse can be approximately calculated by formula  $P_{\text{peak}} = E/t_p$  ( $E$  is the pulse energy,  $t_p$  is the pulse width), and the single-pulse energy instability and pulse width instability of the 5000 pulses can be calculated by formula  $\pm(X_{\text{max}} - X_{\text{min}}) \times 0.5/X_{\text{average}}$  ( $X$  is the pulse energy or pulse width). At the maximal pump current of 110 A and the corresponding pump voltage of 43 V, the main output parameters of the cavity-dumped 1123 nm laser were measured and calculated at repetition rates of 1 kHz, 700 Hz, 400 Hz and 100 Hz, as shown in Table 1. The peak power of output pulse reached 2.24 MW at 1 kHz. While at 100 Hz, the peak power increased to 9.73 MW, which is close to the optical damage threshold of the EO crystal MgO: LN. Therefore, the lower limit of the pulse repetition rate was set at 100 Hz in the experiment. The spectral line width at different pulse repetition rates is about 0.23 nm, and the measured spectrum at 1 kHz is shown in Figure 4.

At the maximum pump current of 110 A, the measured waveforms of the single pulse at different repetition rates are shown in Figures 5(a)–5(d), and corresponding instabilities

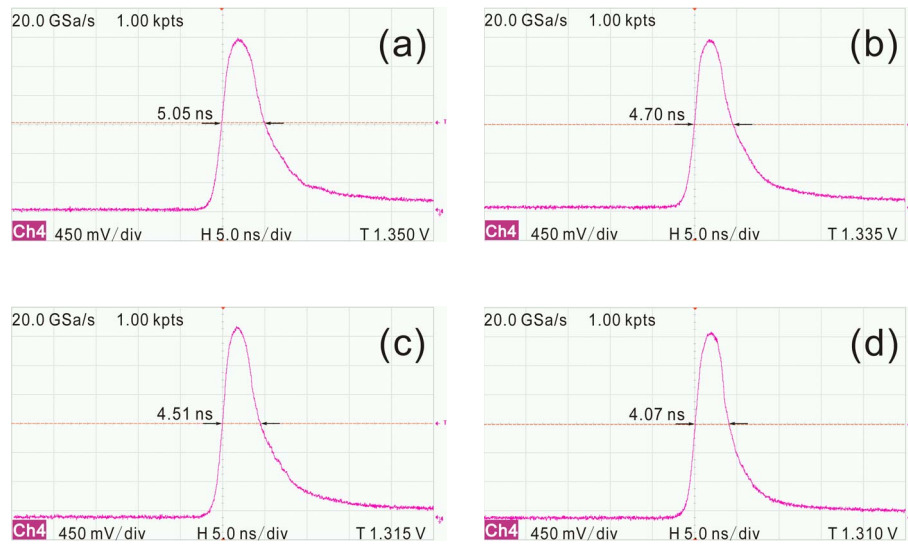


**Figure 5.** Output single-pulse waveforms at repetition rates of (a) 1 kHz, (b) 700 Hz, (c) 400 Hz, and (d) 100 Hz.

**Table 1.** Main output parameters of the cavity-dumped laser under the maximum pump current of 110 A.

Repetition rate	Maximum single-pulse energy	Pulse width	Peak power	Instability of pulse width	Instability of single-pulse energy
1.0 kHz	11.3 mJ	5.05 ns	2.24 MW	$\pm 2.65\%$	$\pm 3.47\%$
700 Hz	18.3 mJ	4.70 ns	3.89 MW	$\pm 2.41\%$	$\pm 3.14\%$
400 Hz	26.9 mJ	4.51 ns	5.96 MW	$\pm 1.75\%$	$\pm 2.59\%$
100 Hz	39.6 mJ	4.07 ns	9.73 MW	$\pm 1.55\%$	$\pm 2.06\%$

of the pulse width are shown in Table 1. The measured pulse width was slightly larger than the round-trip time in the cavity ( $2L/c$ ). The reason is that the rising edge of the EO switch has a small increase and it is larger than the round-trip time ( $2L/c$ ) with the increase of pulse repetition rate. The output pulse width was determined by the rising edge of the EO switch. The corresponding instabilities of the single-pulse energy are also shown in Table 1, which demonstrates that the output pulses have good stability. Reasons for such phenomenon are that a time interval between two adjacent pulses is significantly longer than the upper-level lifetime (about 230  $\mu$ s) of the ceramic Nd: YAG at 1123 nm. This allows the LD array enough time to pump the ceramic Nd: YAG rod, so that the energy gain of each laser pulse could be restored to the maximum. This always maintains a balance between consumption and increase of the inverted populations in the amplification process of stimulated radiation, so that the adjacent laser pulses do not affect each other in the oscillation process. However, the heat accumulation in the EO crystal comes to unneglected as the increase of repetition rate because the EO crystal temperature was not controlled in the experiment. More serious depolarization induced by thermal birefringence results in the reduction of the polarization degree. The turn-off time of the EO crystal is prolonged, and pulse trailing edge time is stretched. When the pulse repetition rate is increased from 100 Hz to 1 kHz,

the pulse width is broadened, and instabilities of the pulse width and the single-pulse energy slightly increase.

In addition, as shown in Figures 6(a) and 6(b), the beam quality, and the 2D and 3D far-field intensity distributions of the 1123 nm pulse laser beam were measured without attenuation using a laser beam quality analyzer (ModeScan1740, Photon Inc.) at the maximum output energy and the pulse repetition rate of 1 kHz. The  $M^2$  factor was measured to be  $M_x^2 = 4.223$ ,  $M_y^2 = 4.510$ , the far-field divergence angle was measured to be  $\theta_x = 3.75$  mrad,  $\theta_y = 3.58$  mrad, and corresponding beam waist size was  $d_x = 1526.03$   $\mu$ m,  $d_y = 1707.31$   $\mu$ m. The results show that the optimization design of the double concave-mirror folded cavity is helpful to improve the laser beam quality of the cavity-dumped lasers.

#### 4. Conclusion

In conclusion, by using pulsed LD side-pumped ceramic Nd: YAG rod and an MgO: LN crystal EO modulator in a double concave-mirror folded cavity, a simple and efficient cavity-dumping method was demonstrated for obtaining 1123 nm laser with high stability, high peak power and narrow pulse width. By optimizing the design, the cavity-dumped lasers were insensitive to thermal effect. A 39.6 mJ of maximum single-pulse energy at 100 Hz was

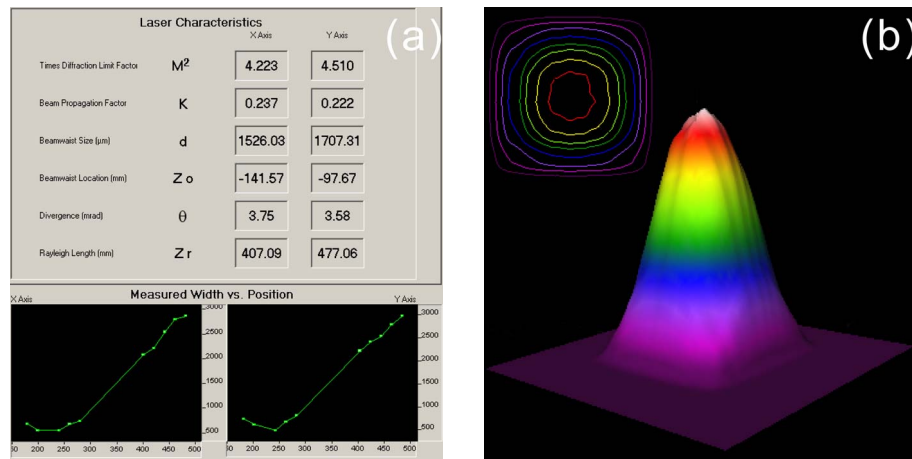


**Figure 6.** Output characteristics of 1123 nm laser beam at 1 kHz. (a) Measured results of the laser beam quality, (b) 3D and 2D (inset) beam energy density distributions.

obtained with a pulse width of 4.07 ns and a peak power of 9.73 MW, corresponding to instabilities of pulse width and single-pulse energy of  $\pm 1.55\%$  and  $\pm 2.06\%$ , respectively. At the maximum repetition rate of 1 kHz, the single-pulse energy was 11.3 mJ with a pulse width of 5.05 ns and a peak power of 2.24 MW, and corresponding instabilities of the pulse width and the single-pulse energy were  $\pm 2.65\%$  and  $\pm 3.47\%$ , respectively. Meanwhile, the beam quality factor ( $M_x^2 = 4.223$ ,  $M_y^2 = 4.510$ ), far-field divergence angle ( $\theta_x = 3.75$  mrad,  $\theta_y = 3.58$  mrad), and beam waist size ( $d_x = 1526.03 \mu\text{m}$ ,  $d_y = 1707.31 \mu\text{m}$ ) were measured, respectively. The experimental results demonstrated above provide promising reference for expanding the scope of 1123 nm laser applications in laser ranging, laser remote sensing, laser medicine and nonlinear optical frequency conversion.

### Acknowledgements

The research was supported by the National Natural Science Foundation of China (No. 61205114) and the Key Laboratory Project – scientific research plan of Shaanxi Provincial Department of Education (No. 2010JS112). Yang Bai and Bing Bai contributed equally to this work.

### References

1. S. T. Hendow and S. A. Shakir, *Opt. Express* **18**, 10188 (2010).
2. A. C. Butler, D. J. Spence, and D. W. Coutts, *Appl. Phys. B* **109**, 81 (2012).
3. C. J. Jin, D. Li, Y. Bai, Z. Y. Ren, and J. T. Bai, *Laser Phys.* **25**, 045802 (2015).
4. D. Teixidor, I. Ferre, J. Ciurana, and T. Ozel, *Robot. Comput.-Integr. Manuf.* **29**, 209 (2013).
5. R. Lehneis, A. Steinmetz, J. Limpert, and A. Tünnermann, *Opt. Lett.* **38**, 2478 (2013).
6. J. H. Lu, J. R. Lu, T. Murai, K. Takaichi, T. Uematsu, J. Q. Xu, K. Ueda, H. Yagi, T. Yanagitani, and A. A. Kaminskii, *Opt. Lett.* **27**, 1120 (2002).
7. J. C. Chen, J. Li, J. L. Xu, W. B. Liu, Y. Bo, X. Q. Feng, Y. Xu, D. L. Jiang, Z. Z. Chen, Y. B. Pan, Y. D. Guo, B. Yan, C. Guo, L. Yuan, H. T. Yuan, Y. Y. Lin, Y. S. Xiao, Q. J. Peng, W. Q. Lei, D. Cui, and Z. Y. Xu, *Opt. Laser Technol.* **63**, 50 (2014).
8. G. Salamu, F. Jipa, M. Zamfirescu, and N. Pavel, *Opt. Express* **22**, 5177 (2014).
9. Y. Tan, H. Zhang, C. J. Zhao, S. Akhmedaliev, S. Q. Zhou, and F. Chen, *Opt. Lett.* **40**, 637 (2015).
10. D. Y. Chen, H. Pan, R. P. Yan, X. Yu, J. Li, Y. F. Ma, X. D. Li, Y. B. Pan, and J. Gao, *Opt. Quantum Electron.* **48**, 1 (2016).
11. H. Rao, Z. J. Liu, Z. H. Cong, Q. J. Huang, Y. Liu, S. S. Zhang, X. Y. Zhang, C. Feng, Q. P. Wang, L. Ge, and J. Li, *Laser Phys. Lett.* **14**, 045801 (2017).
12. E. Raikonen, O. Kimmelma, M. Kaivola, and S. C. Buchter, *Opt. Commun.* **281**, 4088 (2008).
13. R. Paschotta, N. Moore, W. A. Clarkson, A. C. Tropper, D. C. Hanna, and G. Maze, *IEEE J. Sel. Top. Quantum Electron.* **3**, 1100 (1997).
14. S. Lehmann and J. Bosenberg, *Advances in Atmospheric Remote Sensing with Lidar* (Springer, Berlin Heidelberg, 1997), p. 309.
15. W. Telford, M. Murga, T. Hawley, R. Hawley, and B. Packard, *Cytometry Part A* **68**, 36 (2005).
16. J. Gao, X. J. Dai, L. Zhang, H. X. Sun, and X. D. Wu, *J. Opt. Soc. Am. B* **30**, 95 (2013).
17. W. M. Yao, J. Gao, L. Zhang, J. Li, Y. B. Tian, Y. F. Ma, X. D. Wu, G. F. Ma, J. M. Yang, Y. B. Pan, and X. J. Dai, *Appl. Opt.* **54**, 5817 (2015).
18. P. Li, X. H. Chen, H. N. Zhang, B. M. Ma, and Q. P. Wang, *Appl. Phys. Express* **4**, 0927021 (2011).
19. J. X. Bai, P. Li, X. H. Chen, and B. H. Liu, *Appl. Phys. Express* **10**, 082701 (2017).
20. C. L. Sung, C. Y. Lee, C. C. Chang, H. C. Liang, and Y. F. Chen, *Opt. Lett.* **42**, 302 (2017).
21. Y. F. Ma, X. D. Li, X. Yu, R. P. Ren, R. G. Fan, J. B. Peng, X. R. Xu, Y. C. Bai, and R. Sun, *Appl. Opt.* **53**, 3081 (2014).
22. X. S. Liu, Z. H. Shi, Y. T. Huang, Z. W. Fan, J. Yu, J. Zhang, and L. Q. Hou, *Opt. Commun.* **336**, 273 (2015).

23. Y. F. Ma, J. W. Zhang, H. Li, and X. Yu, *Laser Phys. Lett.* **9**, 561 (2012).
24. Y. F. Chen and Y. P. Lan, *Appl. Phys. B* **79**, 29 (2004).
25. X. H. Zhen, L. C. Zhao, and Y. H. Xu, *Appl. Phys. B* **76**, 655 (2003).
26. Y. X. Sun, Y. Bai, D. Li, L. Hou, B. Bai, Y. Z. Gong, L. L. Yu, and J. T. Bai, *Opt. Express* **25**, 21037 (2017).
27. X. B. Wang, X. J. Xu, X. Li, and Q. S. Lu, *Appl. Opt.* **46**, 5237 (2007).
28. Z. N. Zhang, Y. Bai, G. Z. Lei, B. Bai, Y. X. Sun, M. X. Hu, C. Wang, and J. T. Bai, *Laser Phys. Lett.* **13**, 125402 (2016).
29. R. P. Shi, Y. Bai, M. Qi, X. M. Chen, H. D. Wei, Z. Y. Ren, and J. T. Bai, *Laser Phys. Lett.* **11**, 025001 (2014).